

# Strong Screening of Localized Charged Perturbations in Metallic Nanotubes: Effects of Massive Bands

K. Sasaki<sup>1</sup>, A. A. Farajian<sup>2</sup>, H. Mizuseki<sup>2</sup>, and Y. Kawazoe<sup>2</sup>

<sup>1</sup> *Department of Physics, Tohoku University, Sendai 980-8578, Japan*

<sup>2</sup> *Institute for Materials Research, Tohoku University, Sendai 980-8577, Japan*

(Dated: February 23, 2019)

The massive-band effects on screening behavior of metallic carbon nanotubes are theoretically investigated using two different methods; continuous and lattice quantum field theories. Both approaches show strong screening of a localized external perturbation, with a screening length of the order of the nanotube diameter. By calculating the local deformation of the density of massive electron/hole states, the difference in their screening behavior is clarified.

Quantum mechanical behavior of the electrons in carbon nanotubes (CNT's [1, 2]) is mainly governed by the strong Coulomb interactions [3, 4, 5]. Several aspects of the Coulomb interaction are already seen in some experiments of charging [6] and of temperature dependent resistivity [7] which are consistent with current understanding of low-energy excitations in metallic CNT's. The low-energy excitations in the metallic CNT's are theoretically modeled by *massless* bands (linear dispersion bands) with the Coulomb interaction [3, 4, 5]. However when we consider very localized perturbation, it is not clear if the low energy theories describe the physics correctly. Because short distance physics corresponds to high energy, *massive* bands (other sub-bands except the massless bands) would come into dynamics [8]. From the application point of view, understanding the response of CNT's to localized perturbations (e.g., individual dopant atoms) is crucial as it provides the extents of the depletion region in nanotube-based electronic devices. In this letter, taking massive band effects explicitly into account, we focus on the screening of an external charge localized on the surface of the metallic CNT's.

The high-energy excitations can in principle affect the screening phenomena through two different mechanisms; adding massive-fermions loop corrections to the interactions of massless bands and direct interaction of massive bands (non-perturbative effect of the massive bands). Two methods to deal with these mechanisms are investigated. One is a quantum field theoretical method dealing with the massless bands and the one-dimensional long-range Coulomb interaction [9], with one-loop vacuum polarization correction by the massive bands. The other is a lattice model employing a fully self-consistent tight-binding approach [10]. It is the purpose of the present work to compare the results of these two different methods and investigate the true origin of the screening in CNT's. Especially we shall compare the induced charge distribution around the external charge.

Let us begin with the quantum (continuous) field theoretical approach to the screening effect. The  $\pi$ -electrons in CNT's are described by two-component fermion fields  $\psi_{Ns}$  specified by the band index  $N (\in \{1, \dots\})$  and spin  $s (\in \{\uparrow, \downarrow\})$ . The Hamiltonian density of this system is given by  $\mathcal{H} = \mathcal{H}_F + \mathcal{H}_C$  where  $\mathcal{H}_F$  is the free (unper-

turbed) part and  $\mathcal{H}_C$  is the perturbed part including the Coulomb interactions. If we include only tight-binding interactions, then  $\mathcal{H}_F = \sum_{Ns} \mathcal{H}_N$  where

$$\mathcal{H}_N = \psi_{Ns}^\dagger V_\pi \begin{pmatrix} 0 & z(k_x^N, \hat{k}_y) \\ z^*(k_x^N, \hat{k}_y) & 0 \end{pmatrix} \psi_{Ns}. \quad (1)$$

$V_\pi$  is the hopping integral,  $\hat{k}_y = -i\partial_y$  is the wave vector along the tubule axis, the wave vector around the circumference  $ak_x^N = -\frac{2\pi}{\sqrt{3}} + \frac{2a}{d}N$  is discretized by the periodic boundary condition where  $d$  is the diameter of the CNT and  $a$  is the nearest-neighbor C-C spacing. Here we take the case of metallic zigzag CNT's in which the maximum number of  $N$  is  $N_0$  (number of hexagons along the circumference); armchair case is analyzed similarly. The function  $z(k_x, k_y)$  is given by  $z(k_x, k_y) = \sum_i e^{ik \cdot u_i}$ . The vector  $u_i$  is a triad of vectors pointing in the direction of the nearest neighbors of a carbon site [9]. The free Hamiltonian densities  $\mathcal{H}_{N_0/3}$  and  $\mathcal{H}_{5N_0/3}$  describe massless fermions (electrons in massless bands) and the others are for massive fermions in the metallic zigzag CNT. The energy eigenvalues of  $\mathcal{H}_N$  are given by  $\pm V_\pi |z(k_x^N, k_y)|$  which reproduce a standard band structure [2]. These fermions interact with each other via the long-range Coulomb interaction:

$$\mathcal{H}_C = \frac{1}{2} \int_D J(y) V(y-y') J(y') dy', \quad (2)$$

where  $V(y)$  is the unscreened Coulomb potential that we will specify shortly, and the internal charge density  $J$  is given by the sum of individual fermion densities:  $J = \sum_{Ns} J_{Ns}$  where  $J_{Ns} \equiv \psi_{Ns}^\dagger \psi_{Ns}$ . Here we denote the integral region  $D (= [0 : L])$  and  $L$  is the system length.

Low-energy excitations in metallic CNT's are described by a field theory of four massless fermions interacting with each other and with massive fermions through the long-range Coulomb interaction. The massive fermions modify the Coulomb potential between massless fermions because of the vacuum polarization. The unscreened Coulomb potential along the axis is [4]

$$V(x) = \frac{e^2}{4\pi \sqrt{|x|^2 + d^2 + a_z^2}} \frac{2}{\pi} K \left( \frac{d}{\sqrt{|x|^2 + d^2 + a_z^2}} \right), \quad (3)$$

with  $K(z)$  being the complete elliptic integral of the first kind and  $a_z = 1.3[\text{\AA}]$  a cutoff length which corresponds to the Hubbard coefficient  $U_H = 4V_\pi$  in the lattice model (Eq.6).

The massive fermions modify the Coulomb interaction between massless fermions. We estimate this effect using one-loop perturbation. The modified Fourier component of the Coulomb potential is given by  $\bar{\beta}_n = \frac{\beta_n}{1 - \beta_n T_n}$ , where  $\beta_n$  is the  $n$ -th Fourier component of the unscreened Coulomb potential,  $V(x) = \sum_n \beta_n e^{-i\frac{2\pi n}{L}x}$ , and  $T_n$  in the denominator denotes the one-loop contribution of the *massive* fermions [8]. The massive fermions are observed to weaken the Coulomb interaction among massless fermions as is naturally expected. Because the Coulomb potential is modified by the vacuum polarization effects, the massless fermions interact with each other via the screened Coulomb potential whose Fourier components are given by  $\bar{\beta}_n$ .

An external charge can be included by replacing  $J$  with  $J + J^{ex}$  in the Coulomb interactions (Eq. 2), where  $J^{ex}$  is a c-number whose integral over the nanotube length is equal to the total external charge. Here we take a point external charge distribution which is modeled by  $J^{ex} = \delta(x - x_0)$  where  $x_0$  is the position of the external charge. To calculate the induced charge density, we use self-consistent field approach (SCF) which gives an exact result in the case of strictly linear dispersion relation [11]. In Fig. 1, the induced charge distributions around the external point charge for both the unscreened potential and the screened one are depicted. These are obtained using the following formula [8, 9, 12]:

$$\langle J(x) \rangle = \sum_{n>0}^{n_{\max}} \frac{T_n^{\text{ML}} \bar{\beta}_n}{1 - T_n^{\text{ML}} \bar{\beta}_n} \frac{2}{L} \cos\left(\frac{2\pi n}{L}(x - x_0)\right), \quad (4)$$

where  $T_n^{\text{ML}}$  is the loop amplitude of *massless* bands. It should be noted that the screening length is about the diameter of the nanotube for both cases and is not sensitive to the length of the nanotube [9].

Up to now, only the massive-fermion corrections to the *massless*-band interactions, through the leading terms of vacuum polarization, were considered. We now turn to the *massive*-band effects on the screening phenomena, and investigate the influence of direct massive-band interactions. This is accomplished by using a lattice model to describe the nanotube. The model is essentially a tight-binding one which is generalized by including long-range Coulomb interactions [10, 13].

Within this model, the Hamiltonian of a perfect, infinite nanotube is written as  $H = H_F + H_C$  with

$$H_F = \sum_i \epsilon_i c_i^\dagger c_i + \sum_{\langle i,j \rangle} V_\pi c_i^\dagger c_j, \quad (5)$$

$$H_C = \sum_{ij} \frac{\delta n_j}{\sqrt{r_{ij}^2 + U_H^{-2}}} c_i^\dagger c_i, \quad (6)$$

where  $\epsilon_i$  is the on-site energy and  $U_H$  is the Hubbard parameter used in describing on-site interactions [14, 15].

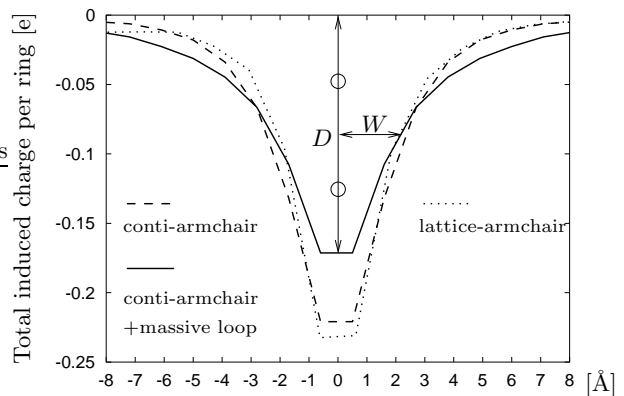


FIG. 1: Total induced charge (including spin degeneracy) along the axis for the (5,5) armchair tube. The dotted line is obtained from the lattice model. The solid and dashed lines are the continuous field theoretical results. The dashed one is for the calculation using unscreened Coulomb potential  $\beta_n$ , and the solid one is for  $\bar{\beta}_n$ . The screening length is about the diameter of the nanotube. Similar results are obtained for the zigzag (9,0) tube.

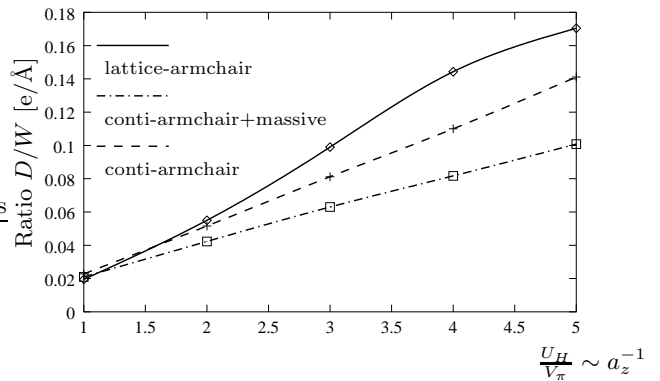


FIG. 2: The cutoff,  $U_H$  (or  $a_z$ ), dependence of a ratio defined by  $D/W$ , where  $D$  is the peak of the induced charge at the position of the external charge and  $W$  is the one-half of the width at the half peak (see Fig. 1). The results show that bigger  $U_H$  (smaller  $a_z$ ) gives smaller screening length. Experimentally,  $U_H$  was reported [16] to be between 2.4 and 4  $V_\pi$ .

Using the experimental estimation of  $U_H$  for carbon [16], we set  $U_H = 4V_\pi$ . The cutoff/ $U_H$  is the only parameter of our model and we examine several cases of  $a_z/U_H$  in this letter. In Eq.6,  $\delta n_i = n_i - n_i^0$  is the change in the self-consistent and screened occupation number  $n_i$  at site  $i$ , as compared to the occupation imposed by external perturbation,  $n_i^0$ . Therefore,  $\delta n_i$  would be the induced charge at site  $i$ , in response to the external perturbation. For a general external perturbation,  $\epsilon_i$  indicates the external bias and/or initial shift of the chemical potential of the bulk nanotube. Here, however, we are concerned with quite localized perturbation, which is modeled by setting  $\epsilon_i = 0$  while modifying  $n_i^0$  as  $n_i^0 \rightarrow n_i^0 + n_i^{ex}$ .

We distinguish three different parts in the infinite nanotube: An unperturbed semi-infinite part to the left, a perturbed finite part in the middle, and an unperturbed semi-infinite part to the right. In the unperturbed parts,  $n_i^0 = 0.5$  (excluding the spin degeneracy) and  $\delta n_i = 0$ . This implies that the length of the perturbed finite part, for which  $\delta n_i$ 's are assumed to be nonzero, is chosen to be long enough such that the external perturbation is fully screened within this part of the nanotube. For concreteness, we assume that the localized external perturbation only modifies the sites of the two carbon rings of the nanotube by adding  $n_i^{ex}$ 's to the corresponding  $n_i^0$ 's. (A ring consists of all the carbon atoms with the same longitudinal coordinate along the nanotube axis.) The two rings with nonzero  $n_i^{ex}$ 's are assumed to be at the middle of the perturbed finite part of the nanotube, which, in turn, is taken to consist of 16 carbon rings. This number of carbon rings has proven [10] to be long enough in order to derive the converged induced charges, as increasing the number of rings has had no effect on the self-consistent occupations. The self-consistent procedure of calculating the induced charges  $\delta n_i$ 's proceeds as follows [10]: Starting with an initial guess of zero  $\delta n_i$ 's in the Hamiltonian Eq.6, the surface Green's functions of the two semi-infinite unperturbed parts are calculated. These surface Green's functions are then attached to the Green's function of the perturbed middle part of the tube. This way, the local density of states (LDOS), and hence the induced charges can be obtained, which are then used to initialize the Hamiltonian for another round of  $\delta n_i$ 's calculation. This procedure is continued until the induced charges are determined self-consistently. Throughout the self-consistent calculation, the chemical potential of the system is assumed to be that of the unperturbed nanotube, as after screening the whole system would be in thermal equilibrium and would have a unique chemical potential. Furthermore, the external perturbation being localized and finite, the unique chemical potential would be that of the unperturbed semi-infinite parts of the nanotube, which act like reservoirs attached to the perturbed finite part.

As specific examples, an armchair (5,5) and a zigzag (9,0) nanotube are considered, whose diameters are 6.78 and 7.04 [Å]. The external perturbation of the middle two rings of the perturbed part of these tubes are defined as  $n_i^{ex} = 0.0250$  and  $n_i^{ex} = 0.0278$ , for the armchair and zigzag tubes, respectively. This external perturbation amounts to adding a total charge of  $1.0e$  to the middle two rings for both the armchair and the zigzag tubes.

The resultant induced charges for the (5,5) armchair tube are depicted in Fig. 1. It is observed that the screening length is of the order of the nanotube diameter, in all the different calculations. The screening length also depends on the cutoff  $a_z$  or the Hubbard coefficient  $U_H$ . The cutoff dependence of induced charge pattern is plotted for several  $U_H$  values in Fig. 2. The main features of the induced charge pattern were observed to hold for the whole range of experimentally reported  $U_H$  [16]. From

Fig. 1 we further see that the induced charges obtained by including only the massless bands in the continuous field-theoretical calculation are in qualitative agreement with the results of lattice calculation, which, in addition to the massless bands, includes the effects of direct massive bands interactions. Interestingly, including the massive-loop corrections to massless bands interactions does not result in better agreement with the results of lattice model. This suggests that, within the continuous model, the massive-loop corrections to the massless band interactions somehow cancel the effects of direct massive band interactions, such that the results of a calculation based only on massless bands turn out to be in agreement with the results of the lattice model. In other words, in the continuous approach, the induced charge density is given by the sum of two densities as  $\langle J \rangle = \langle J_{\text{massless}} \rangle + \langle J_{\text{massive}} \rangle$  where  $\langle J_{\text{massless}} \rangle$  is defined in Eq.4.  $\langle J_{\text{massive}} \rangle$  is an induced charge density due to massive bands themselves, and is what we have ignored. Perturbative inclusion of massive bands reduces the peak of the former charge density and results in a more appreciable difference with the lattice results. Considering overall agreement of the lattice results and continuous field theoretical results based on the massless bands, it is natural to expect that the  $\langle J_{\text{massive}} \rangle$  partially cancels the perturbative effects of the massive bands on the massless bands interaction, such that the net induced charge density is decided by the massless bands only.

In addition to the calculations for the armchair tube, we have performed similar calculations on the (9,0) zigzag tube. The results of the continuous model [11] show the same features, as those of the armchair one, when compared to the results of lattice model. This indicates that the agreement between the continuous massless results and lattice results is not accidental. It is remarkable that in both the continuous and lattice calculations the peak value of the induced charge shows a reduction of  $\sim 15\%$ , when one compares zigzag results with armchair results.

In order to see the LDOS deformation and the effects of massive bands more clearly, we show the self-consistent LDOS's for a typical unperturbed site (solid line), a site located at one of the rings perturbed externally (dashed line), and a site, of the perturbed portion of the nanotube, located at the furthest ring relative to the middle two rings (dotted line). The latter site indicates the border between the perturbed finite part of the tube and one of the unperturbed semi-infinite parts. In Fig. 3, enlarged typical regions of the electron (hole) LDOS's are depicted. It is clearly seen that the densities of massive states in the perturbed region are different from the corresponding densities of the unperturbed region. However, as one expects, the difference is much more pronounced near the location of external perturbation than far from it. In fact, the border LDOS shows how the extremely perturbed LDOS near the external perturbation transforms rather smoothly, as one moves toward the border of the perturbed region, into the unperturbed LDOS. Another very interesting feature is the

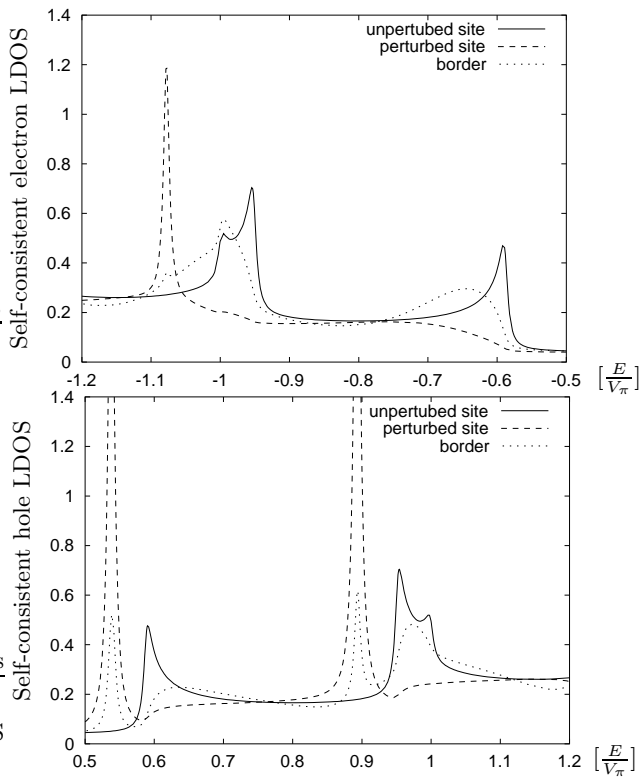


FIG. 3: Self-consistent electron (top) and hole (bottom) LDOS. Fermi energy is located at zero.

difference in the behavior of the electron states as compared to the hole states. For the external perturbation mentioned above, namely *addition* of one extra electron

to the middle two rings, it is seen that the hole states tend to accumulate at lower energies, while the electron states are pushed toward higher energies. This indicates the decisive effect of the Coulomb interactions among the massive fermion- (both electron- and hole- ) states. One should notice that, due to the rotational symmetry selection rule [10], the electron/hole states belonging to a certain band are not allowed to jump over to another band with higher/lower energy. But *within each band* the electron states tend to concentrate at higher energies, and the hole states tend to concentrate at lower energies. This is indeed the reason for the enhanced/decreased densities at band edges.

In summary, we have analyzed the charge screening in metallic nanotubes using two different methods, including explicitly the massive bands effects, based on lattice and continuous field theoretical models. In both methods, a localized external charge is shown to be screened with a small screening length about the diameter of the tube. The local density of states, calculated by the lattice model, indicates that the massive bands are strongly affected by the external charge. As for the continuous field theoretical model, we have included the massive bands (perturbative) loop corrections in massless bands interactions. Although non-perturbative effects of massive bands were not considered, the results show basically the same pattern as that of the lattice model results. This shows that the perturbative corrections of massive bands are partially cancelled by the induced charge due to massive bands themselves. The short screening length reported here makes it possible, at least theoretically, to achieve nanoscale integration of nanotube-based electronic devices.

- 
- [1] S. Iijima, *Nature*, **354**, 56 (1991).  
[2] R. Saito *et al.*, *Physical Properties of Carbon Nanotubes* (Imperial College Press, London, 1998).  
[3] C. Kane *et al.*, *Phys. Rev. Lett.* **79**, 5086 (1997).  
[4] R. Egger and A. O. Gogolin, *Phys. Rev. Lett.* **79**, 5082 (1997); *Eur. Phys. J. B* **3**, 281 (1998).  
[5] H. Yoshioka and A.A. Odintsov, *Phys. Rev. Lett.* **82**, 374 (1999).  
[6] S.J. Tans *et al.*, *Nature (London)* **386**, 474 (1997); *ibid.* **394**, 761 (1998); H. Postma *et al.*, *J. Low. Temp. Phys.* **118**, 495 (2000).  
[7] M. Bockrath *et al.*, *Nature (London)* **397**, 598 (1999); H. Postma *et al.*, *Science* **293**, 76 (2001).  
[8] M.F. Lin and D.S. Chuu, *Phys. Rev. B* **56**, 4996 (1997). To the best of our knowledge, only Lin *et al.* have considered the massive band effects in metallic nanotubes. Their approach, however, ignores the extension of the  $\pi$ -electrons perpendicular to the nanotube wall. This extension is included in our approach via an effective cutoff/Hubbard parameter.  
[9] K. Sasaki, *Phys. Rev. B* **65**, 155429 (2002); *ibid.* **65**, 195412 (2002).  
[10] A.A. Farajian *et al.*, *Phys. Rev. Lett.* **82**, 5084 (1999); A.A. Farajian *et al.*, *Phys. Rev. B* **65**, 165415 (2002).  
[11] K. Sasaki *et al.*, arXiv:cond-mat/0207149.  
[12] We set  $n_{\max}$  equal to  $L/\sqrt{3}a$  for the armchair CNT. This cutoff may cause an oscillatory pattern [9] of the induced charge density for the Coulomb interaction with shorter cutoff length  $a_z$ .  
[13] K. Harigaya and S. Abe, *Phys. Rev. B* **49**, 16746 (1994).  
[14] F. Liu, *Phys. Rev. B* **52**, 10677 (1995).  
[15] K. Esfarjani and Y. Kawazoe, *J. Phys. Condens. Matter* **10**, 8257 (1998).  
[16] R.G. Pearson, *Inorg. Chem.* **27**, 734 (1988).